Tuneable Stiffness Design of Soft Continuum Manipulator

Seri Mastura Mustaza[1(✉)], Duale Mahdi[2], Chakravarthini Saaj[1], Wissam A. Albukhanajer[1], Constantina Lekakou[2], Yahya Elsayed[2], and Jan Fras[3]

[1] Department of Electronic Engineering, Faculty of Engineering and Physical Sciences, University of Surrey, Guildford, Surrey GU2 7XH, UK
{s.mustaza,c.saaj,w.a.albukhanajer}@surrey.ac.uk
[2] Division of Mechanical, Medical and Aerospace Engineering, Faculty of Engineering and Physical Sciences, University of Surrey, Guildford, Surrey GU2 7XH, UK
{d.a.mahdi,c.lekakou,y.elsayed}@surrey.ac.uk
[3] Przemyslowy Instytut Automatyki i Pomiarow, Al. Jerozolimskie 202, 02-486 Warsaw, Poland
jfras@piap.pl

Abstract. Soft continuum robots are highly deformable and manoeuvrable manipulators, capable of navigating through confined space and interacting safely with their surrounding environment, making them ideal for minimally invasive surgical applications. A crucial requirement of a soft robot is to control its overall stiffness efficiently, in order to execute the necessary surgical task in an unstructured environment. This paper presents a comparative study detailing the stiffness characterization of two soft manipulator designs and the formulation of a dynamic stiffness matrix for the purpose of disturbance rejection and stiffness control for precise tip positioning. An empirical approach is used to accurately describe the stiffness characteristics along the length of the manipulator and the derived stiffness matrix is applied in real-time control to reject disturbances. Further, the capability of the two types of soft robots to reject disturbances using the dynamic control technique is tested and compared. The results presented in this paper provide new insights into controlling the stiffness of soft continuum robots for minimally invasive surgical applications.

Keywords: Stiffness control · Soft continuum robots · Robustness · Minimally invasive surgery

1 Introduction

There is an increasing interest to advance the state-of-the-art of soft robotics in medical applications. This is primarily driven by the need for a robot that can manoeuver in confined spaces and interact with organs and tissue safely, especially, in applications such as minimally invasive surgery (MIS). Numerous research studies have been conducted that demonstrate soft continuum robots for MIS applications [1, 2, 3, 4]. The highly articulated soft robot manipulators are advantageous compared

H. Liu et al. (Eds.): ICIRA 2015, Part III, LNAI 9246, pp. 152–163, 2015.
DOI: 10.1007/978-3-319-22873-0_14

with rigid manipulators because of their low modulus, making them compliant to compressive forces and hence, allowing to manoeuvre easily and safely through narrow orifices and tight passages between organs. However, flexibility of the manipulator also implies low payload capacity and poor distal stiffness. While it is desirable for the manipulator to be gentle when interacting and manoeuvring within its surroundings, significant stiffness is required once the robot is in place to perform useful surgical tasks.

For a fully operational soft robot, a key requirement is its ability to navigate in an unstructured environment in the presence of perturbation to avoid crude movements and instability of the distal tip. For these reasons, tuneable stiffness is required in order for the manipulator to reject perturbing forces anywhere in the workspace. This can be achieved by tuning the forces generated by the manipulator to compensate the effect of perturbations, thus ensuring safe manoeuvrability and manipulation of the soft robot.

The currently implemented tuneable stiffness methods for soft manipulators require a more complex mechanical design e.g. tendon driven mechanism [5, 6, 7] and granular jamming [7, 8, 9]. While prototypes based on these designs have been proven to provide the desired stiffness, they introduce additional problems. In the case of granular jamming, the granular matter used reduces steerability, while, tendon based mechanisms may introduce undesirable non-linear characteristic to the entire system as well as poor disturbance rejection [10]. The ideal solution is to design stiffness controller coupled with position estimation algorithm to produce a desired positional tip stiffness. However, assessing the stiffness of soft manipulator can be difficult and stiffness control for this type of manipulator is achieved indirectly from position control without sensing the forces or stiffness at the tip as proposed in [11]. Apart from the work in [11], stiffness control of soft manipulators has been poorly researched and developed.

The goal of this paper is to analyse and compare the stiffness characteristics of two different designs of soft continuum manipulators and use this information for real-time stiffness control by implementing a disturbance rejection algorithm. The empirical approach taken involves characterizing the stiffness of the manipulator through experiments and deriving a relationship between the force exerted by the manipulator and the joint displacement to generate a dynamic stiffness matrix. Disturbance rejection in this study is achieved by directly measuring the perturbing forces on the manipulator and compensating for any deflection using the dynamic stiffness matrix, in contrast to the work in [11] whereby no information on forces was utilized to execute the stiffness control.

This paper is organised into the following sections. Section 2 describes the prototypes of the soft manipulators. Section 3 details the stiffness analysis carried out. Section 4 discusses the relationship between the applied disturbance force at the tip and the change in chamber pressure to compensate for this tip displacement. Finally, Section 5 gives concluding remarks and suggests future work.

2 Soft Continuum Manipulator Prototype

This study investigates the stiffness characteristics of two soft continuum manipulator prototypes as shown in Fig. 1. Both of the prototypes were fabricated using Ecoflex ™ 0050 silicone and are composed of three actuating pressure chambers displaced at 120o apart in symmetrical radial arrangement. Two different braiding structures are explored to maximize the longitudinal extension and bending of the manipulator in achieving the desired steerability. The structural differences between the two prototypes are explained below:

Prototype 1. The first prototype is composed of three equally spaced semi-cylindrical chambers in radial arrangement moulded directly into a single cylindrical unit as shown in Fig. 1(a) [12]. A crimped braided sheath is used around the module to constrain the inflation of the chamber and maximize bending under applied pressure. The diameter of each semi-cylindrical actuating chamber is 8mm and the diameter of the cylindrical unit is 30 mm.

Prototype 2. The second prototype is more compact in structure compared with Prototype 1. It comprises three full-cylindrical actuating pressure chambers without any braided sleeve around the module as illustrated in Fig. 1(b). The radial expansion of the pressure chambers are constrained by tightly wound nylon thread around each individual chamber to maximize the bending and longitudinal expansion. Similar to the first prototype, the actuating chamber is 8mm in diameter and with an overall smaller module diameter of 25mm [13].

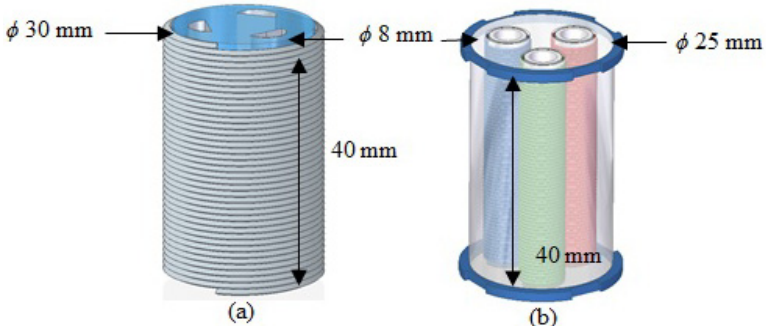

Fig. 1. (a) Prototype 1 (crimped braided sheath) and (b) prototype 2 (nylon threaded chambers)

Both braiding structures effectively minimize the radial expansion of the chambers under actuation, but their behaviours differ tremendously. Prototype 2 is less sensitive to changes in pressure compared to prototype 1. This is due to the internal braiding that restricts changes in chamber length and cross-sectional area. Furthermore, the prototype 2 eliminates cross-talk between chambers and friction between the outer surface of the silicone and the wall of the external braiding which prototype 1 suffers from. More details on the structural design of these prototypes can be found in [12, 13, 14].

3 Stiffness Analysis

This section investigates and compares the stiffness characteristics of the two prototypes presented in Section 2. The stiffness matrix for each module is derived and used to control the stiffness of the manipulator.

The stiffness matrix is defined as the relationship between the forces exerted to the displacements of all joints [15]:

$$\boldsymbol{F} = \boldsymbol{K}\boldsymbol{d} \tag{1}$$

where $\boldsymbol{F}$ is the force (n dimensional vector) at the tip in (N), $\boldsymbol{d}$ is the displacements of the joints (n dimensional vector) in (m) and $\boldsymbol{K}$ is stiffness matrix in (N/m). Normally, this matrix is a constant throughout its operating workspace and configuration. However, due to the inherent non-linear behaviour of the manipulator, a constant matrix will not properly reflects the changes in the stiffness of the manipulator, hence, will not be effective in controlling the stiffness of the manipulator.

The forces exerted by each actuating chambers is symmetrical around 120 degree and the force sensor [16], [17] used has a symmetry of 90 degree on the x-y coordinate axes, therefore, the relationship between the displacement of each chamber and the forces acting on each chamber cannot be obtained directly. This relationship is obtained indirectly in two steps: first, the relationship between a change in force as a function of a change in pressure is obtained. The second step is to manipulate the relationship in the first step in terms of pressure and substitute this into the Euler-Bernoulli equation to obtain a relationship between displacement, stiffness and pressure.

In this study, the Euler-Bernoulli beam model equation [18] is used. This equation relates a change in length to a change in pressure:

$$\Delta dl_i = \frac{F_p}{EA} dl_i = \frac{dP_i A_{ch}}{EA} dl_i \tag{2}$$

where dl is the length of a small fragment of the chamber in (m), Δdl is the change in length of the chamber due to pressure in (m), $i \in \{1,2,3\}$ is an index used to indicate chamber number, dP is change in pressure in (N/m2), E is the material's Young's Modulus in (N/m2), and A is the cross sectional area of the module in (m2). The pressure in each chamber can be used to calculate the force applied on the module using (3):

$$F = PA_{ch} \tag{3}$$

where A_{ch} is the cross sectional area of the chamber. Table 1 shows the constants in (2) i.e. the Young's Modulus, the cross-sectional area of the module and the chamber cross-sectional area. Figure 2 shows a comparison between the beam model and the experimental data for the two prototypes investigated. The beam model and experimental data correlate for both prototypes and for this reason, the beam model is considered a representative model.

Table 1. Beam model parameters

Parameter	Description	Prototype 1	Prototype 2
E	Young's modulus	40000 N/m^2	178000 N/m^2
A	Manipulator cross-sectional area	4.22e-4 m^2	4.52e-4 m^2
a	Chamber cross-sectional area	2.21e-5 m^2	4.42e-5 m^2

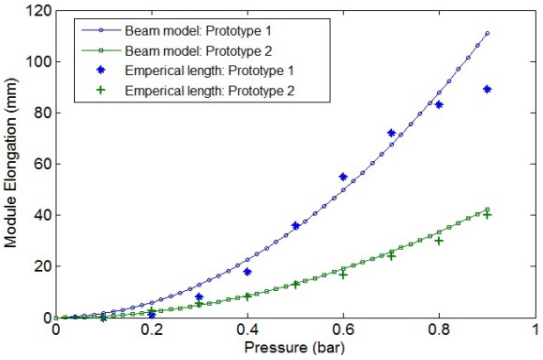

Fig. 2. Relationship between pressure and the change in length for one chamber

To obtain the relationship between change of force and change of pressure, the tip of the manipulator is constrained to emulate interactions with the environment. For a small change in pressure ΔP (see Fig. 3), the forces exerted at the tip of the module are measured using the force sensor developed by Noh et al [17]. This is done across the operational pressure range (up to 0.8 bar) and allows for the characterisation of the stiffness of the manipulator in all operational pressure range and configurations of interest. Thus, the behaviour and pattern between actuated pressure and force exertion for both prototypes is estimated. This analysis gives the relationship between force and pressure, for the three actuating chambers. For example, the change of force as a function of change of pressure relationship for chamber 1 of prototype 1 is governed by (4):

$$\left.\begin{aligned} dF_x &= -4.366dP_1 + 1.6368 \\ dF_y &= -1.7853dP_1 + 0.5973 \\ dF_z &= 1.6199dP_1 - 1.4472 \end{aligned}\right\} \quad (4)$$

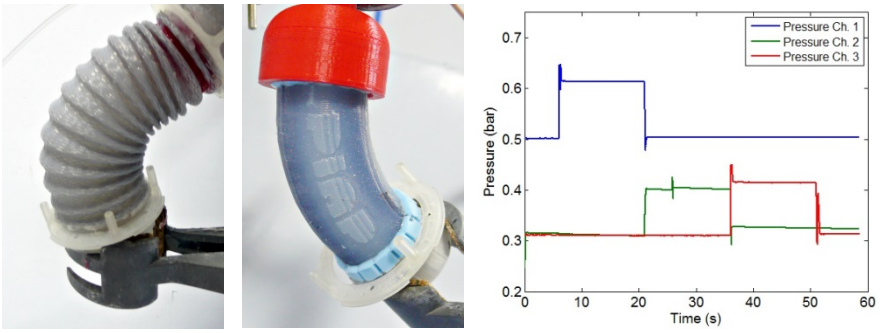

Fig. 3. Experimental setup to evaluate the relationship between pressure and force: (a) and (b) prototype 1 and 2 with constrained tip respectively, (c) input pressure supply to both prototypes

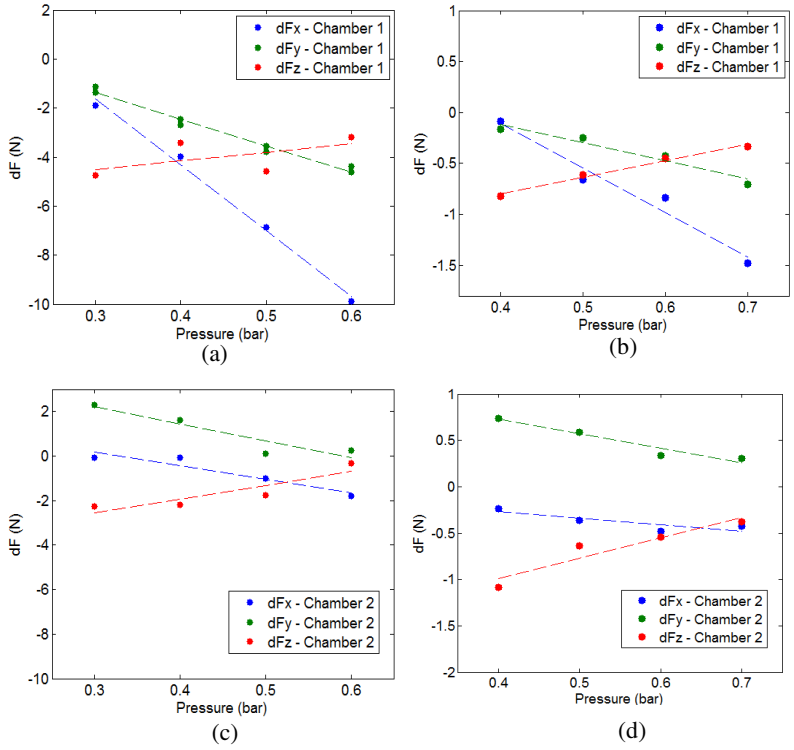

Fig. 4. Linear fitting of the relationship between change in force and pressure: (a) and (c) for prototype 1, (b) and (d) for prototype 2

Figure 4 compares the relationships of the change in force as a function of change in pressure for the two prototype manipulators. The figure shows data for two chambers (out of three), i.e., chamber 1 and 2. As illustrated in these figures, both prototypes have a similar overall trend where the directions of the forces exerted are comparable. However, prototype 1 exerts a significantly higher force compared with pro-

totype 2. This is due to the difference in braiding structure of the manipulator. For small pressure perturbations imposed within each chamber, the external braiding of prototype 1 allows it displace more (see Fig.2) compared with the second prototype. Furthermore, the cross-sectional area of prototype 1 changes as the chamber is actuated causing the resultant force to be higher.

The goal for stiffness control for surgical tasks is to maintain the tip position as forces are exerted at the distal end of the manipulator. The input to the controller is the desired displacement and this is compared with the actual displacement for position control through reducing the position error. The change in length(Δdl), the force (F_P) acting on the chamber is determined empirically at a given position (in the x, y and z directions). The straight line equations obtained in (4) as well as the beam model is utilized to generate the dynamic relationship between length and force as the chambers are pressurized at different levels. The linear equation in (5) is re-written in terms of forces to give (6):

$$dF_{x,y,z} = B_{i,x,y,z}\, dP_i + C_{i,x,y,z} \tag{5}$$

$$dP_i = \frac{dF_{x,y,z} - C_{i,xyz}}{B_{i,xyz}} \tag{6}$$

Substituting (6) into (2) gives the relationship of the desired change is length as given in (7):

$$\Delta dl_i = \left(\frac{dF_{x,y,z} - C_{i,xyz}}{B_{i,xyz}}\right)\frac{A_{ch}}{EA} dl_i \tag{7}$$

which can be generalized as:

$$\Delta d\boldsymbol{l} = \boldsymbol{K}^{-1} d\boldsymbol{F} \tag{8}$$

where $\boldsymbol{K}^{-1}$ is the inverse of stiffness matrix also known as the compliance matrix which take the following form:

$$\boldsymbol{K}^{-1} = \begin{bmatrix} \mathrm{K}_{11}(\mathrm{l}_1) & \mathrm{K}_{12}(\mathrm{l}_1) & \mathrm{K}_{13}(\mathrm{l}_1) \\ \mathrm{K}_{21}(\mathrm{l}_2) & \mathrm{K}_{22}(\mathrm{l}_2) & \mathrm{K}_{23}(\mathrm{l}_2) \\ \mathrm{K}_{31}(\mathrm{l}_3) & \mathrm{K}_{32}(\mathrm{l}_3) & \mathrm{K}_{33}(\mathrm{l}_3) \end{bmatrix}. \tag{9}$$

4 Disturbance Rejection

For a given operating scenario, the manipulator could experience unknown interaction forces at the tip which result in the deflection of the tip from its desired working point. This could have a detrimental effect in practice, possibly resulting in unintended interaction between the tip and its surroundings resulting in tissue damage. This deflection can be effectively compensated for by directly measuring the interaction forces in-situ and utilizing the compliance matrix derived in (9) to maintain the desired tip position.

The deflection and tip position of the manipulator (X_c, Y_c, Z_c) is measured using the NDI Aurora sensor [19]. To maintain the desired position in the presence of disturbance forces, the inverse kinematic model in [20] is utilized to calculate the desired joint position.

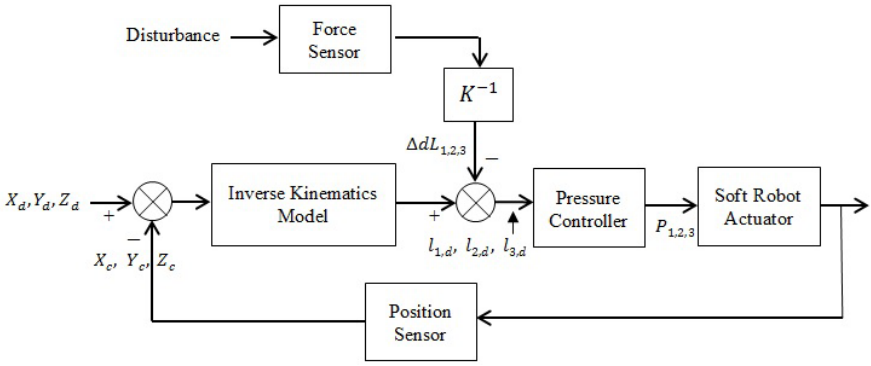

Fig. 5. Position control architecture through stiffness control and disturbance rejection

In the current test setup, disturbances are injected by applying arbitrary forces on the tip of the manipulator. Based on the measured forces, the system calculates the resulting $\Delta dl_{1,2,3}$ using (8) and re-calculates the desired chamber length $(l_{1,d}, l_{2,d}, l_{3,d})$ to overcome this disturbance. The controller then outputs the appropriate pressure, $P_{1,2,3}$, to achieve the desired length. The overall control architecture based on the inverse kinematic developed in [20] is as shown in Fig. 5.

Figure 6 illustrates the disturbance forces applied at the tip, the deflection of the tip due to this disturbance and the corresponding chamber pressure to counteract these disturbances for both prototypes. For prototype 1, disturbance forces in the range of 0.6 to 0.7 N are applied for a period of 7.5 seconds (Fig. 6(a)) which results in tip deflection in the range of 3 to 5 mm. For prototype 2, a steeper disturbance forces in the range of 0.8 to 1 N were applied for a period of 3.5 seconds (Fig. 6(b)) resulting in larger tip deflection between 2 to 5.5 mm. Larger disturbance forces were applied to prototype 2 because of its inherent structural stability resulting from the internal nylon threading. To counteract these disturbance forces, the controller utilizes the dynamic stiffness matrix to estimate the resultant change in length due to these disturbance forces and applies pressure in the relevant chambers to maintain the tip at the desired position. As can be seen in Fig. 6(e) and Fig. 6(f), the controller manages to keep the deflection of the tip to within 2 to 5.5mm and nullifies the displacement caused by the disturbances force applied at the tip of manipulator. Both prototypes successfully reject the disturbance but prototype 2 takes a longer time to achieve this. This was attributed to the difference in duration and magnitude of the disturbance force applied to the two prototypes. For both prototypes, corrective pressures in the range of 0.15 to 0.3 bar were applied. Figure 7 shows the results in the absence of the dynamic stiffness control without force feedback, whereby huge deflections in the range of 10 to 20 mm are observed. Comparing results in Fig. 6 and Fig. 7 confirms that a dynam-

ic stiffness matrix is required in order to actively counteract disturbance forces for real-time applications. Further, the controller responds in real-time to maintain tip position at the desired position under perturbed conditions, thus proving the robustness of the stiffness controller.

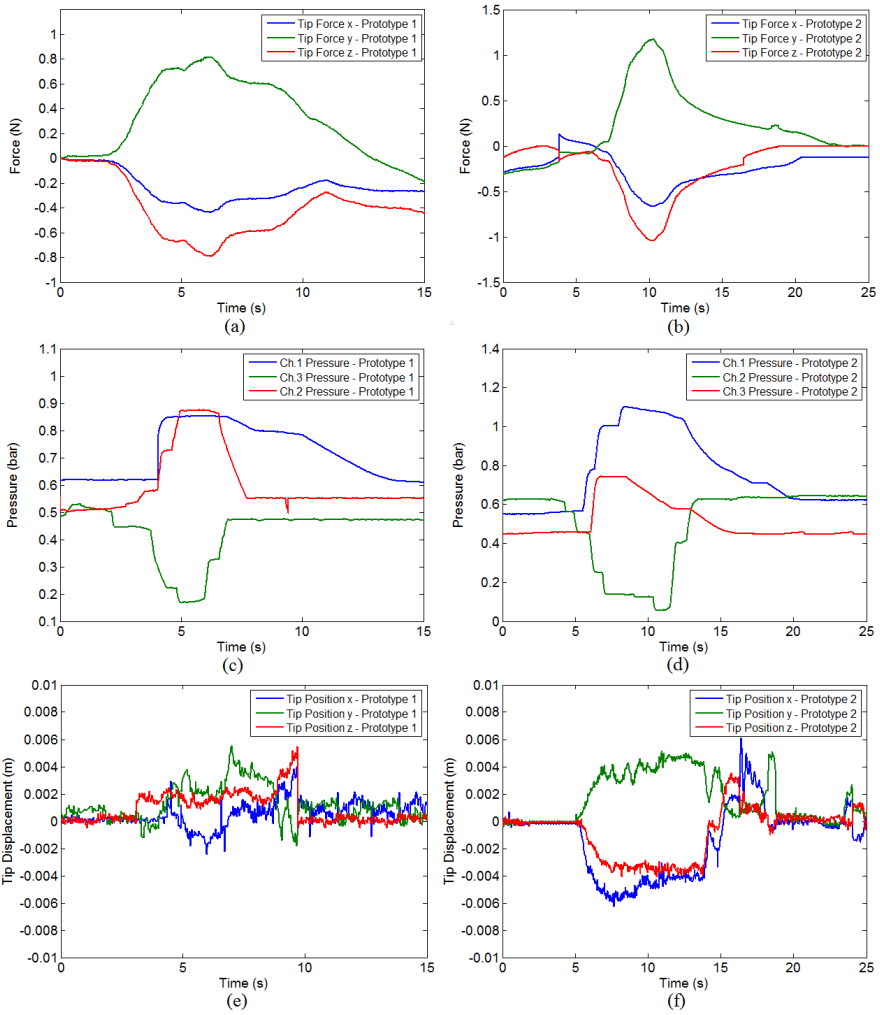

Fig. 6. Position control with force feedback for disturbance rejection and stiffness control (a) disturbance force at tip of manipulator, (c) pressure actuation to compensate the disturbance and (e) displacement of tip for prototype 1. Similarly (b, d and f) are the corresponding plots for prototype 2

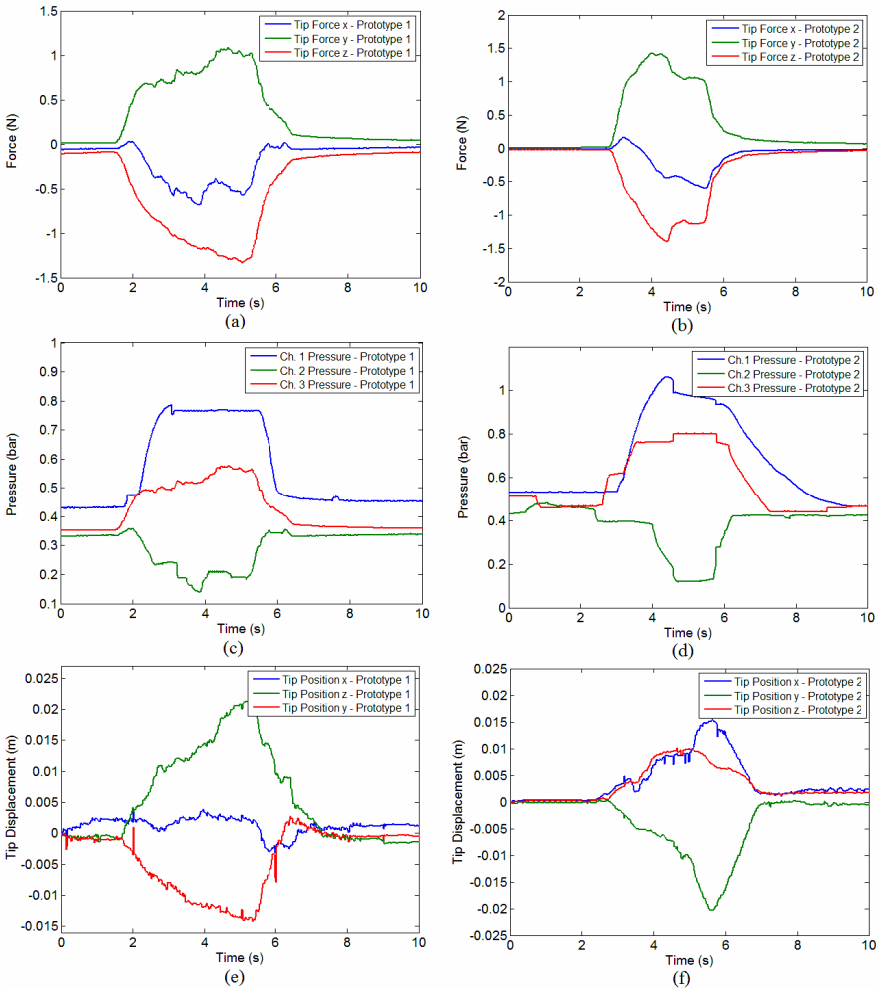

Fig. 7. Position control with no force-feedback: (a) disturbance force at tip of manipulator, (c) pressure actuation to compensate the disturbance and (e) displacement of tip for prototype 1. Similarly (b, d and f) are the corresponding plots for prototype 2

5 Conclusion and Future Work

The experimental results suggest that the two designs of the soft continuum robot modules have significantly different stiffness, re-enforcing the need for a separate dynamic stiffness matrix tailored for each system. The results covered in this paper show that the empirically derived stiffness matrix is suitable for disturbance rejection in real-time control. More investigation is required to develop a generalized stiffness matrix suitable for a class of soft continuum robots. Further research is under way to achieve a complete characterization that covers the entire workspace of interest for different designs of soft continuum robots.

Acknowledgement. The work described in this paper is supported by the STIFFFLOP project grant from the European Commission's Seventh Framework Programme under grant agreement 287728. This project is also partly supported by the Ministry of Education Malaysia, Universiti Kebangsaan Malaysia (UKM). We thank the following members of the STIFF-FLOP consortium for providing us with various building blocks of the integrated system architecture: Anthony Remazeilles from Tecnalia, Toni Oliver Duran and Ugo Cupcic from Shadow Robot Company, Matthias Mende and Erwin Gerz from the University of Siegen, Dr. Tao Geng who was previously with the University of Surrey and Zbigniew Nawrat and Kamil Rohr from the Foundation for Development of Cardiac Surgery.

References

1. Simaan, N., Taylor, R., Flint, P.: A dexterous system for laryngeal surgery. In: IEEE International Conference on Robotics and Automation, vol. 1, pp. 351–357, April 2004
2. Sears, P., Dupont, P.: A steerable needle technology using curved concentric tubes. In: IEEE/RSJ International Conference on Intelligent Robots and Systems, pp. 2850–2856, October 2006
3. Cianchetti, M., Ranzani, T., Gerboni, G., Nanayakkara, T., Althoefer, K., Dasgupta, P., Menciassi, A.: Soft robotics technologies to address shortcomings in today's minimally invasive surgery: the STIFF-FLOP approach. Soft Robotics **1**(2), 122–131 (2014)
4. Elsayed, Y., Lekakou, C., Ranazani, T., Cianchetti, M., Morino, M., Chirurgia, M., Arezzo, M., Gao, T., Saaj, C.: Crimped braided sleeves for soft, actuating arm in robotic abdominal surgery. Minimally Invasive Therapy & Allied Technologies (2015). doi: 10.3109/13645706.2015.1012083
5. Stilli, A., Wurdemann, H.A., Althoefer, K.: Shrinkable, stiffness-controllable soft manipulator based on a bio-inspired antagonistic actuation principle. In: IEEE/RSJ International Conference on Intelligent Robots and Systems, pp. 2476-2481, September 14-18, 2014. doi:10.1109/IROS.2014.6942899
6. Maghooa, F., Agostino, S., Althoefer, K., Wurdemann, H.A.: Tendon and pressure actuation for a bio-inspired manipulator based on an antagonistic principle. In: IEEE International Conference on Robotics and Automation (ICRA), Seattle, USA, May 26–30, 2015
7. Cheng, N.G., Lobovsky, M.B., Keating, S.J., Setapen, A.M., Gero, K.I., Hosoi, A.E., Iagnemma, K.D.: Design and analysis of a robust, low-cost, highly articulated manipulator enabled by jamming of granular media. In IEEE International Conference on Robotics and Automation, pp. 4328–4333, May 2012
8. Loeve, A.J., van de Ven, O.S., Vogel, J.G., Breedveld, P., Dankelman, J.: Vacuum packed particles as flexible endoscope guides with controllable rigidity. IGranular Matter **12**(6), 543–554 (2010)
9. Jiang, A., Xynogalas, G., Dasgupta, P., Althoefer, K., Nanayakkara, T.: Design of a variable stiffness flexible manipulator with composite granular jamming and membrane coupling. In: IEEE/RSJ International Conference on Intelligent Robots and Systems (IROS), pp. 2922–2927, October 7-12, 2012
10. Lee, Y.-T., Choi, H.-R., Chung, W.-K., Youm, Y.: Stiffness control of a coupled tendon-driven robot hand. IEEE Control Systems **14**(5), 10–19 (1994). doi:10.1109/37.320882
11. Mahvash, M., Dupont, P.: Stiffness control of surgical continuum manipulators. IEEE Transactions on Robotics **27**(2), 334–345 (2011)
12. Lekakou, C., Elsayed, Y., Geng, T., Saaj, C.M.: Skins and Sleeves for Soft Robotics: Inspiration from Nature and Architecture. Advanced Engineering Materials (2015). doi:10.1002/adem.201400406

13. Fraś, J., Czarnowski, J., Maciaś, M., Główka, J., Cianchetti, M., Menciassi, A.: New STIFF-FLOP module construction idea for improved actuation and sensing. In: IEEE International Conference on Robotics and Automation (ICRA), Seattle, USA, May 26-30, 2015
14. Cianchetti, M., Ranzani, T., Gerboni, G., De Falco, I., Laschi, C., Menciassi, A.: STIFF-FLOP surgical manipulator: mechanical design and experimental characterization of the single module. In: IEEE International Conference on Intelligent and Robotic Systems, pp. 3567-3581 (2014)
15. Carbone, G.: Stiffness analysis for grasping tasks: grasping in robotics. In: Carbone, G., (ed.) Mechanisms and Machine Science, vol. 10, pp. 17–55. Springer, London (2013)
16. Noh, Y., Secco, E.L., Sareh, S., Wurdemann, H., Faragasso, A., Back, J., Liu, H., Sklar, E., Althoefer, K.: A continuum body force sensor designed for flexible surgical robotic devices. In: 36th Annual International Conference of IEEE Engineering in Medicine and Biology Society (EMBC), pp. 3711−3714 (2014)
17. Noh, Y., Sareh, S., Back, J., Wurdemann, H.A., Ranzani, T., Secco, E.L., Faragasso, A., Liu, H., Althoefer, K.: A three-axial body force sensor for flexible manipulators. In: IEEE International Conference on Robotics and Automation (ICRA), pp. 6388−6393 (2014)
18. Fraś, J., Czarnowski, J., Maciaś, M., Główka, J.: Static Modeling of Multisection Soft Continuum Manipulator for Stiff-Flop project. Springer (2014)
19. NDI 3D measurement technology systems. http://www.ndigital.com/medical/products/aurora/
20. Calinon, S., Bruno, D., Malekzadeh, M.S., Nanayakkara, T., Caldwell, D.G.: Human-robot skills transfer interfaces for a flexible surgical robot. Computer Methods and Programs in Biomedicine **116**(2), 81–96 (2014)